




# Star Log-extended eMulation: a method for efficient computation of the Tolman-Oppenheimer-Volkoff equations

Sudhanva Lalit <sup>1,\*</sup> Alexandra C. Sempowski <sup>2,†</sup> and Joshua M. Maldonado <sup>2,‡</sup>

<sup>1</sup>*Facility for Rare Isotope Beams, Michigan State University, East Lansing, MI 48824, USA*

<sup>2</sup>*Department of Physics and Astronomy and Institute of Nuclear and Particle Physics, Ohio University, Athens, OH 45701, USA*

(Dated: November 21, 2024)

We emulate the Tolman-Oppenheimer-Volkoff (TOV) equations, including tidal deformability, for neutron stars using a novel hybrid method based upon the Dynamic Mode Decomposition (DMD) for the first time. This method, which we call Star Log-extended eMulation (SLM), utilizes the underlying logarithmic behavior of the differential equations to enable accurate emulation of the nonlinear system. We show predictions for well-known phenomenological equations of state (EOS) with fixed parameters and with a freely-varying parametric Quarkyonic EOS. Our results produce a significant computational speed-up of  $\approx 3 \times 10^4$  compared to high fidelity calculations using standard Runge-Kutta methods. Hence, this provides an efficient emulator for the numerous TOV evaluations required by multi-messenger astrophysical frameworks that infer constraints on the EOS from neutron star mergers. The ability of the SLM algorithm to learn a mapping between parameters of the EOS and subsequent neutron star properties also opens up potential extensions for assisting in computationally prohibitive uncertainty quantification (UQ) for any type of EOS. The source code for the methods employed in this work will be openly available in a public GitHub repository for community modification and use.

*Introduction.*—The advent of multi-messenger astronomy, accelerated by LIGO’s gravitational wave measurements [1–3] and NICER’s pulsar observations [4–8], has coincided perfectly with advances in Bayesian uncertainty quantification (UQ) in nuclear physics [9, 10] and the FRIB era of experiment [11]. These three complementary approaches enable a refined understanding of the strong interaction, which governs matter from finite nuclei to dense, stellar compact objects, e.g., neutron stars. The lack of direct probes into the interior composition of neutron star cores indicates we must rely on the combination of information from neutron-star observations and binary mergers, nuclear experiment [12, 13], and the construction of state-of-the-art nuclear potentials to infer the equation of state (EOS) of the star [14–16]. This thermodynamic description is then propagated through the Tolman-Oppenheimer-Volkoff (TOV) equations [17, 18] to determine the corresponding mass and radius of neutron-rich matter. Future gravitational wave (GW) measurements, as well as data from NICER and Cosmic Explorer, will provide more constraints on this mass-radius relationship, including other important properties, e.g., tidal deformability [19–23], which will, in turn, allow us to place tighter constraints on the EOS.

This multi-messenger era of astrophysics has led to the need for more efficient calculations of the TOV equations due to their use in large-scale frameworks, e.g., LIGO’s GW inference framework [24–26], where thousands of solutions can be required for reliable UQ of the mass-radius posterior. The precision era of nuclear physics [16, 27–31] has also led to the use of smaller-scale Bayesian frameworks that require sampling of the EOS and the computation of posteriors for neutron star properties [16, 30, 32, 33], hence necessitate numerous

solutions to the TOV equations. To perform these calculations efficiently, the computational burden of solving the TOV equations, especially when including tidal deformability, must be overcome. An approach already employed in nuclear physics is the design and use of sophisticated emulators to reduce computational time and resources. Recent efforts in constructing model-intrusive, projection-based emulators have produced remarkable results in nuclear scattering [34–38], and model-extrusive emulators such as Gaussian processes (GPs) have been used successfully in nuclear astrophysics [30, 39].

In this Letter, we present a novel emulation strategy based upon the Dynamic Mode Decomposition (DMD) method used in analyses of time dynamics [40–43], which, to differentiate from standard DMD, we call Star Log-extended eMulation (SLM). Currently available DMD libraries [44] are incapable of handling the nonlinearity of the TOV equations; hence, this work establishes an emulator that is able to overcome this hurdle. We apply two state-of-the-art SLM emulators to the TOV equations, including tidal deformability, for the first time. We begin by benchmarking the emulator against high fidelity solutions to these equations. We then employ two versions of this emulation strategy: one to nonparametric, e.g., tabular EOSs, and another for parametric EOSs, to a two-parameter Quarkyonic EOS. The latter learns a mapping between EOS parameters and previously mentioned neutron star properties, a necessary feature for the Bayesian calibration of other phenomenological EOSs with freely varying parameters. Our emulators, along with the code to produce the results in this Letter, will be publicly available for community use [46].

*Neutron star properties.*—Macroscopic properties of neutron stars, including mass, radius, and tidal deforma-

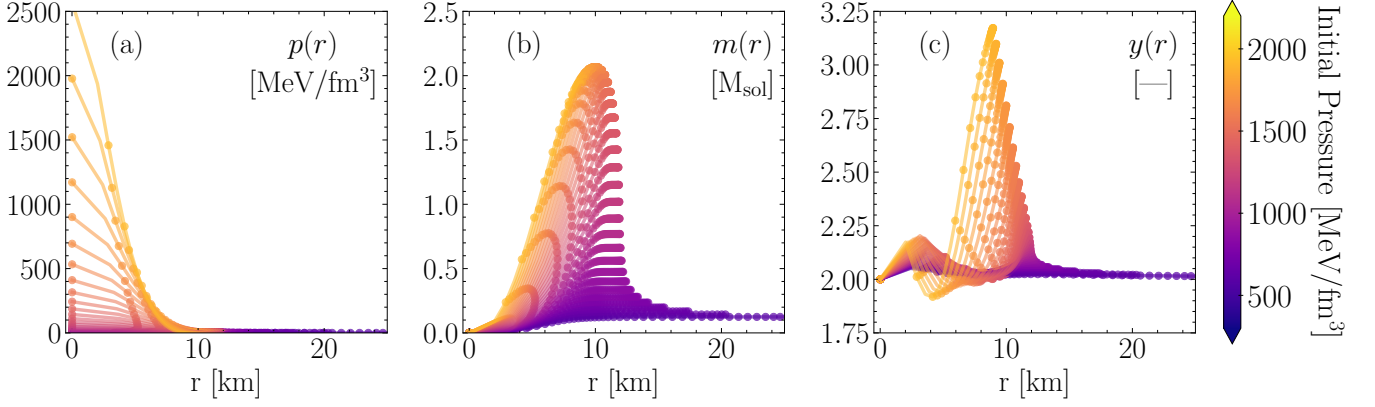


FIG. 1. Solutions to the TOV and tidal deformability coupled differential equations (solid curves) for the SLy4 tabular EOS [45], and the corresponding SLM predictions (dotted curves). These results highlight the ability of the SLM routine to capture the underlying structure of the nonlinear differential equations.

bilities can be determined by solving the TOV equations simultaneously with appropriate differential equations corresponding to each additional desired quantity. We use the scaled TOV equations [47] and scale the differential equation for tidal deformability [20–22] in a similar fashion.

The resulting equations are

$$\frac{dp}{dx} = -\frac{1}{2} \frac{(\varepsilon(x) + p(x)) (m(x) + 3x^3 p(x))}{x^2 (1 - m(x)/x)} \quad (1)$$

$$\frac{dm}{dx} = 3x^2 \varepsilon(x) \quad (2)$$

$$\frac{dy}{dx} = -\frac{y(x)^2}{x} - \frac{F(x)y(x)}{x} - \frac{Q(x)}{x} \quad (3)$$

with

$$F(x) = \left[1 - \frac{3}{2}(\varepsilon(x) - p(x))\right] [1 - m(x)/x]^{-1}, \quad (4)$$

and

$$Q(x) = \frac{\frac{3}{2}x^2}{\left(1 - \frac{m(x)}{x}\right)} \left[ 5\varepsilon(x) + 9p(x) + \frac{\varepsilon(x) + p(x)}{c_s^2(x)} - \frac{4}{x^2} \right] - \left( \frac{m(x)/x + 3x^2 p(x)}{\left(1 - \frac{m(x)}{x}\right)} \right)^2,$$

where  $p(x)$ ,  $\varepsilon(x)$ ,  $m(x)$  and  $c_s(x)$  are the scaled dimensionless pressure, energy density, mass and speed-of-sound functions respectively, while  $y(x)$  is the scaled solution to the tidal equation. As can be seen from equations (1)–(3), the dense matter EOS is the essential input to this system, as well as the initial conditions to ensure physical conditions, e.g.,  $p(x) \rightarrow 0$  at the edge of the star. We solve these equations simultaneously to obtain masses, radii, and tidal deformabilities,  $\Lambda$ , of neutron stars using a high-fidelity (HF) fourth order Runge-Kutta (RK4) solver. We also construct the dimensionless coefficient,  $k_2$ , known as the Love number [22].

As input to the TOV solver, we have chosen EOSs that can obtain a maximum mass of greater than  $2M_\odot$ , possess different sets of underlying parameters, and enable us to test our algorithm on a variety of masses and radii, as well as various structures of the Love number curve,  $k_2(R)$ . Our HF solutions for maximum masses and corresponding radii are presented in Table I, and are consistent with the results in the compOSE database [45].

*Star Log-extended eMulation (SLM).*—Existing model-extrusive emulators, such as DMDs, are appealing to consider for use in emulating the TOV equations. DMD-based emulators are generally applicable to problems that have either polynomial nonlinearities or can be expressed as an eigenvalue problem [34, 35, 38, 55], and are used extensively for emulation of various time-dependent systems [40, 56–58]. A recent work applied DMDs to nonlinear problems [59]; however, the DMD algorithms presented there suffer from the inability to capture the more complex nonlinear dynamics of the coupled TOV system. To overcome this limitation, we extend the methods of Ref. [40] for time-independent systems with underlying logarithmic structure.

In the standard DMD algorithm, one desires to find a family of surrogate equations for a given system of coupled, time-dependent differential equations. In our case, we solve a similar system of equations, which can be written as

$$\frac{\partial y}{\partial r} = \mathcal{F}(y(\mathbf{x}, r)), \quad (5)$$

where  $\mathcal{F}$  is a nonlinear operator that describes the governing equation of interest by discretizing the phase space, i.e., taking snapshots at discrete values of  $r$ . Here  $r$  is the independent variable, e.g., scaled radius, while  $\mathbf{x}$  consists of other dependent variables such as  $\varepsilon$ . We therefore wish to find

$$\frac{dy}{dr} = \hat{\mathbf{A}}\mathbf{y}, \quad (6)$$

EOS	HF		SLM		Error (%)		Time (s)	
	Max. Mass [ $M_\odot$ ]	Radius [km]	Max. Mass [ $M_\odot$ ]	Radius [km]	Max. Mass	Radius	HF	SLM
Tabular EOS								
SLy4	2.067	10.033	2.068	10.033	0.02	0.00	9.218	$2.135 \times 10^{-4}$
APR	2.193	9.979	2.194	9.982	0.05	0.03	9.237	$2.149 \times 10^{-4}$
FSU Garnet	2.054	10.998	2.068	11.000	0.66	0.02	9.226	$2.319 \times 10^{-4}$
BL	2.083	10.194	2.085	10.204	0.10	0.11	9.246	$2.099 \times 10^{-4}$
DS-CMF-5	2.023	11.896	2.026	11.647	0.17	2.09	9.228	$2.215 \times 10^{-4}$
Quarkyonic EOS								
$\Lambda=300.00, \kappa=0.19$	2.947	14.763	2.917	14.666	1.00	0.66	9.286	$3.822 \times 10^{-4}$
$\Lambda=352.63, \kappa=0.14$	2.653	12.512	2.675	12.561	0.83	0.39	9.299	$4.051 \times 10^{-4}$
$\Lambda=405.26, \kappa=0.10$	2.441	11.199	2.441	11.063	0.40	1.21	9.234	$4.361 \times 10^{-4}$
$\Lambda=447.37, \kappa=0.28$	2.294	10.462	2.294	10.463	0.01	0.01	9.292	$4.261 \times 10^{-4}$
$\Lambda=500.00, \kappa=0.23$	2.226	10.180	2.221	10.177	0.22	0.03	9.156	$3.898 \times 10^{-4}$

TABLE I. Comparisons of the HF and emulated maximum mass and corresponding radii for various EOSs selected from the compOSE database [45], as well as the same quantities computed for the Quarkyonic EOS [54] with various choices of parameters  $\Lambda$  and  $\kappa$ . The tabular EOSs are emulated using the SLM algorithm (see Fig. 2), whereas the Quarkyonic EOS is emulated through the pSLM algorithm (see Fig. 3). The remarkable efficiency achieved is seen in the large difference between the time spent computing the emulated and HF solutions (last two columns), leading to an average speed-up of  $2.95 \times 10^4$ .

where the linear operator  $\hat{\mathbf{A}}$  approximates the dynamics of the system. The operator  $\hat{\mathbf{A}}$ , a finite approximation of the infinite dimensional Koopman operator, is learned in a data-driven fashion.

Since Eq. (5) lacks time dependence, it does not fit into the general class of problems that DMD can be directly applied to. Thus, in the DMD procedure, we replace the independent variable  $t$  with the linear index of the data in the training set, and include the independent variable  $r$ , e.g., the scaled radius, in the set of snapshots. We perform the DMD algorithm for the logarithm of the chosen snapshots, i.e.,  $\log r$ ,  $\log p(r)$ ,  $\log m(r)$  and  $\log y(r)$ , due to the logarithmic manifestation of the nonlinearities in the system. We employ the formalism of extended DMDs in Ref. [60] to modify the data to make it suitable for our calculations, e.g., by utilizing polynomial extensions of the general DMD algorithm (see the supplemental material [61] for more details). Instead of using the solutions to Eqs. (1)-(3) for the SLM routine, one can also consider the neutron star mass  $M(R)$ , radius  $R$ , central pressure  $P_{\text{central}}(R)$  and  $k_2(R)$  (see Fig. 2) and follow the same procedure above.

*Parametric-SLM.*—The parametric-SLM (pSLM) method is based upon the reduced Eigen-Pair Interpolation method (rEPI) from Ref. [40], using our modified, time-independent snapshots. However, instead of using a point-wise Lagrange interpolation, we use a recently developed technique based on the Greedy Recombination Interpolation Method (GRIM) for Banach spaces (B-GRIM) [62] to interpolate within the parameter space, as this method is optimal for high-dimensional spaces where residual minimization in Banach spaces is effective. This is especially true when dealing with noisy data or requiring iterative improvement of the solution, whereas Lagrange interpolation is unstable

in such cases. In this method, the objective is to construct an interpolant that minimizes the norm ( $\ell^1$ ) in that space. In the greedy recombination method, the algorithm iteratively selects basis elements to improve the interpolation, minimizing the error at each step.

In our case, pSLM allows us to find the relation between the parameters of the EOS to the neutron star properties described by the solutions to the TOV equations through a modification to Eq. (6),

$$\frac{d\mathbf{y}^\theta}{dr} = \hat{\mathbf{A}}(\boldsymbol{\theta})\mathbf{y}^\theta, \quad (7)$$

where  $\boldsymbol{\theta}$  is a vector of parameters corresponding to the prediction set. Thus, pSLM can be employed to predict at parameters that have not been used to train the emulator (see the supplemental material [61] for the full pSLM algorithm).

*Results.*—Fig. 1 shows the solutions to Eqs. (1)-(3) as functions of radius  $r$  and the output from the SLM algorithm for each quantity, respectively. The emulator is able to recover the solutions from the HF solver, allowing for accurate predictions between HF solutions. Hence, SLM only needs a few solutions of each quantity to reliably reconstruct the HF results. Fig. 2 then shows SLM applied to the HF solutions of  $M - R$ ,  $P_{\text{central}} - R$ , and  $k_2 - R$  curves for the chosen tabular EOSs and the respective relative errors between the HF and emulated results, found to be  $\approx 10^{-3}$ . With an average speed of about  $2.2 \times 10^{-4}$  seconds, compared to the HF average speed of  $\approx 9.2$  seconds, the SLM routine is shown to be remarkably efficient. This proof-of-principle calculation also indicates that SLM can be used to accurately recover the structure of each curve through prediction between HF solutions corresponding to a given EOS. Table I shows the numerical results for the maximum masses and cor-

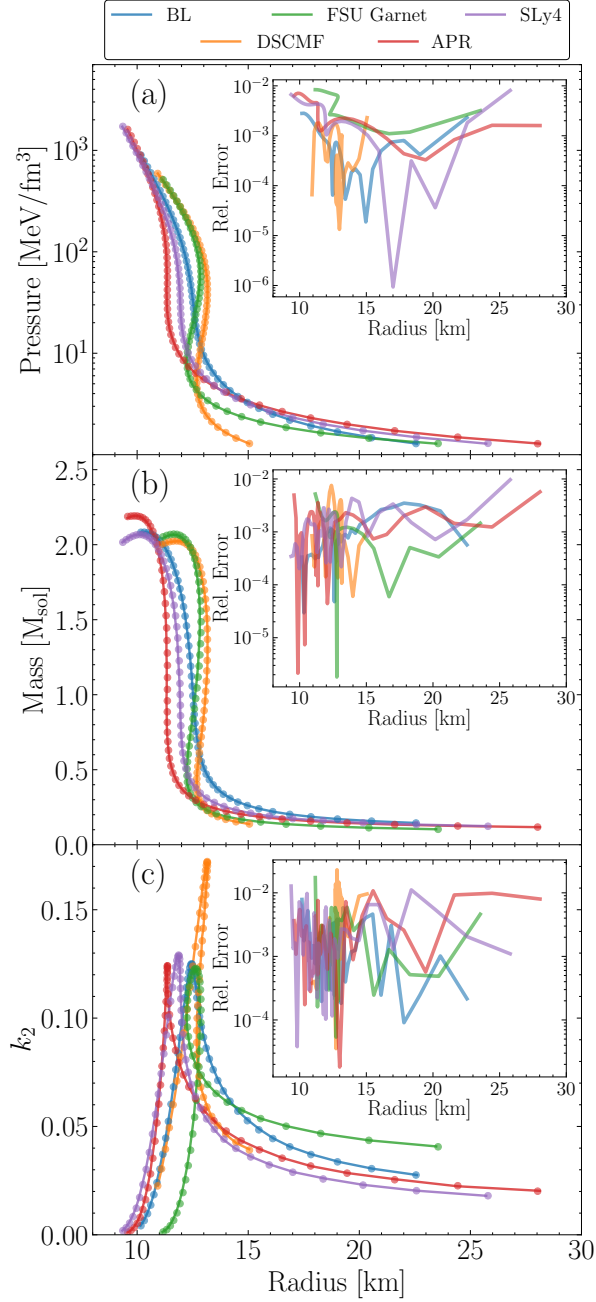


FIG. 2. (a) Central pressure, (b) mass, and (c) dimensionless Love number  $k_2$  as functions of radius. These properties are calculated for five tabular EOSs [48–53]. The dots (solid lines) indicate SLM (HF) results. The inset shows the relative error between the HF and SLM results.

responding radii calculated from the HF solver for these EOSs, the same quantities using the SLM algorithm, and the subsequent percent error between the HF and emulated calculations. All errors are  $\leq 1\%$  for the maximum mass, and  $< 3\%$  for the corresponding radii.

We use the Quarkyonic EOS to test the pSLM algorithm, varying parameters  $\Lambda$  and  $\kappa$  over a range of

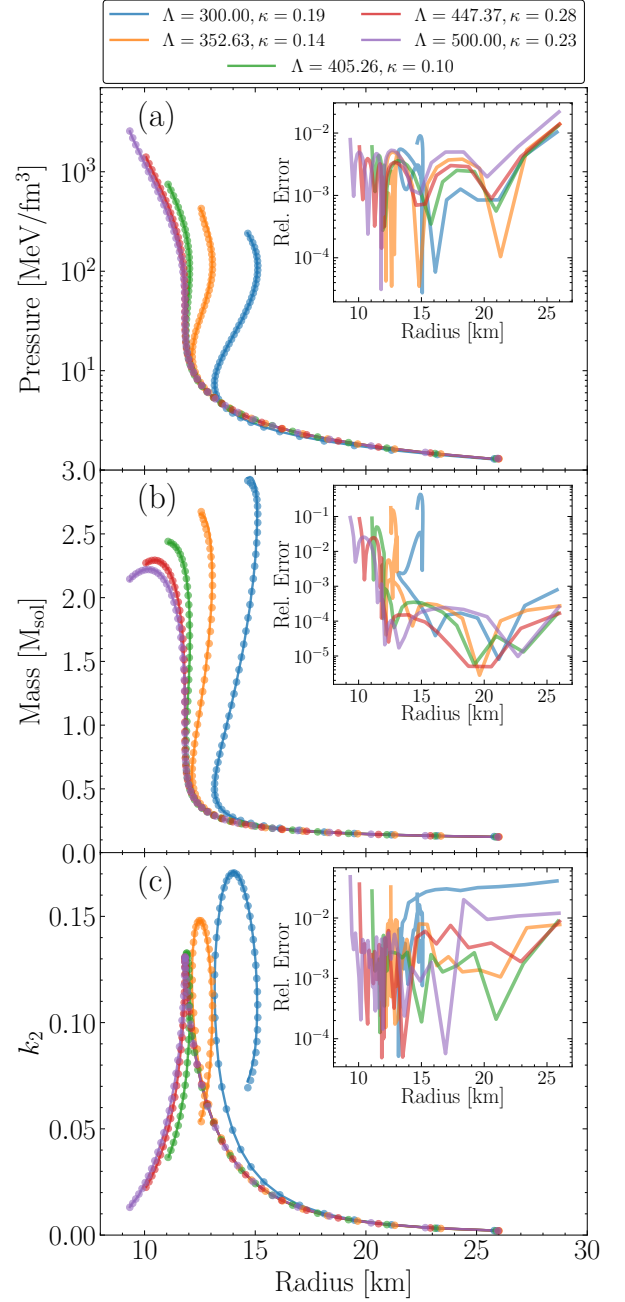


FIG. 3. (a) Central pressure, (b) mass, and (c) dimensionless Love number  $k_2$  as function of radius for the Quarkyonic EOS [54] using pSLM, with varying parameters  $\Lambda$  and  $\kappa$ . The result shown here is the prediction for a given test parameter set that has not been used to train the emulator. The dots (solid lines) indicate SLM (HF) results.

300 – 500 MeV and 0.1 – 0.3, respectively. The training set is composed of 15 datasets consisting of radii, central pressures, masses and Love numbers. Using pSLM we predict the curves for test parameter sets as shown in Fig. 3, which were not used to train the emulator. The maximum mass and radius results from the HF solver



and the pSLM emulator, as well as the percent error and speed of the calculation, are also recorded in Table I. The average speed for the pSLM emulator is  $\approx 4.1 \times 10^{-4}$  seconds, yielding an overall speed up of  $\approx 4.5 \times 10^4$  over the HF method. All percent errors are  $\leq 1\%$  for all maximum masses and radii.

*Summary and outlook.*—In this work, we presented SLM as a method to emulate the TOV equations, including tidal deformabilities. We employed SLM to emulate  $M-R$  curves from tabular EOSs, such as the well-known SLy4 EOS. We then used a parametric version of SLM to emulate EOSs that possess an arbitrary number of parameters. In particular, we focused on the Quarkyonic EOS. The results from these emulators agree well with HF RK4 evaluations of the TOV equations. We gain an average computational speed-up of  $\sim 3 \times 10^4$  across both types of EOSs considered; hence, both SLM algorithms present highly efficient emulators for large-scale computations of the TOV equations in scenarios such as those presented by multi-messenger astrophysical inference frameworks. This emulation strategy will help to reduce the bottleneck that the TOV equations present in such calculations, without sacrificing necessary accuracy. The algorithm is not limited to small parameter sets, and as such can be easily generalized to EOSs with larger parameter sets. More broadly, the SLM algorithm works well for problems that possess logarithmic dependence in the solutions. Hence, our work can be straightforwardly extended in future to problems that share this trait, e.g., density functionals with non-affine parameter dependence. To help other researchers utilize and build upon our work, the code pertaining to our SLM algorithm and the generation of the results in this Letter, as well as tutorials to assist new users, will be published in a public GitHub repository for the use of the scientific community [46].

*Acknowledgments.*—We thank Jérôme Margueron for a careful review of our manuscript, Xilin Zhang for engaging discussions, Amy L. Anderson for providing the FSUGarnet data, and CompOSE (<https://compose.obspm.fr>) for providing all other tabular EOS datasets. A.C.S. thanks the Facility for Rare Isotope Beams for their hospitality and encouragement during the completion of this work. This work is supported by the CSSI program, Award OAC-2004601 (BAND collaboration [63]) (A.C.S.), and the U.S. Department of Energy, Office of Science, Nuclear Physics, under Award DE-SC0023688 (S.L.), Award DE-FG02-93-40756 (A.C.S.) and Award DE-SC0024233 (STREAMLINE collaboration) (J.M.M.).

---

\* [lalit@frib.msu.edu](mailto:lalit@frib.msu.edu)

† [as727414@ohio.edu](mailto:as727414@ohio.edu)

- ‡ [jm998521@ohio.edu](mailto:jm998521@ohio.edu)
- [1] B. P. Abbott *et al.* (LIGO Scientific, Virgo), *Phys. Rev. Lett.* **119**, 161101 (2017), [arXiv:1710.05832 \[gr-qc\]](#).
  - [2] B. P. Abbott *et al.* (LIGO Scientific, Virgo), *Phys. Rev. Lett.* **121**, 161101 (2018), [arXiv:1805.11581 \[gr-qc\]](#).
  - [3] B. P. Abbott *et al.* (LIGO Scientific, Virgo), *Astrophys. J. Lett.* **892**, L3 (2020), [arXiv:2001.01761 \[astro-ph.HE\]](#).
  - [4] M. C. Miller *et al.*, *Astrophys. J. Lett.* **887**, L24 (2019), [arXiv:1912.05705 \[astro-ph.HE\]](#).
  - [5] M. C. Miller *et al.*, *Astrophys. J. Lett.* **918**, L28 (2021), [arXiv:2105.06979](#).
  - [6] T. E. Riley *et al.*, *Astrophys. J. Lett.* **887**, L21 (2019), [arXiv:1912.05702 \[astro-ph.HE\]](#).
  - [7] T. E. Riley *et al.*, *Astrophys. J. Lett.* **918**, L27 (2021), [arXiv:2105.06980](#).
  - [8] D. Choudhury *et al.*, *Astrophys. J. Lett.* **971**, L20 (2024), [arXiv:2407.06789 \[astro-ph.HE\]](#).
  - [9] D. R. Phillips, R. J. Furnstahl, U. Heinz, T. Maiti, W. Nazarewicz, F. M. Nunes, M. Plumlee, M. T. Prato, S. Pratt, F. G. Viens, and S. M. Wild, *J. Phys. G* **48**, 072001 (2021), [arXiv:2012.07704 \[nucl-th\]](#).
  - [10] J. A. Melendez, R. J. Furnstahl, D. R. Phillips, M. T. Prato, and S. Wesolowski, *Phys. Rev. C* **100**, 044001 (2019), [arXiv:1904.10581](#).
  - [11] B. A. Brown *et al.*, (2024), [arXiv:2410.06144 \[nucl-th\]](#).
  - [12] A. Sorensen *et al.*, *Prog. Part. Nucl. Phys.* **134**, 104080 (2024), [arXiv:2301.13253](#).
  - [13] R. Kumar *et al.* (MUSES), (2023), [arXiv:2303.17021](#).
  - [14] C. Drischler, J. W. Holt, and C. Wellenhofer, *Annu. Rev. Nucl. Part. Sci.* **71**, 403 (2021), [arXiv:2101.01709](#).
  - [15] J. M. Lattimer, *Ann. Rev. Nucl. Part. Sci.* **71**, 433 (2021).
  - [16] H. Koehn *et al.*, (2024), [arXiv:2402.04172 \[astro-ph.HE\]](#).
  - [17] R. C. Tolman, *Physical Review* **55**, 364 (1939).
  - [18] J. R. Oppenheimer and G. M. Volkoff, *Physical Review* **55**, 374 (1939).
  - [19] K. S. Thorne and A. Campolattaro, “Non-Radial Pulsation of General-Relativistic Stellar Models. I. Analytic Analysis for  $L \geq 2$ ,” (1967).
  - [20] T. Hinderer, *Astrophys. J.* **677**, 1216 (2008), [Erratum: *Astrophys. J.* 697, 964 (2009)], [arXiv:0711.2420 \[astro-ph\]](#).
  - [21] T. Hinderer, B. D. Lackey, R. N. Lang, and J. S. Read, *Phys. Rev. D* **81**, 123016 (2010), [arXiv:0911.3535 \[astro-ph.HE\]](#).
  - [22] S. Postnikov, M. Prakash, and J. M. Lattimer, *Phys. Rev. D* **82**, 024016 (2010), [arXiv:1004.5098 \[astro-ph.SR\]](#).
  - [23] C. C. Moustakidis, T. Gaitanos, C. Margaritis, and G. A. Lalazissis, *Bulg. J. Phys.* **44**, 093 (2017).
  - [24] P. T. H. Pang *et al.*, *Nature Commun.* **14**, 8352 (2023), [arXiv:2205.08513 \[astro-ph.HE\]](#).
  - [25] R. Abbott *et al.* (KAGRA, VIRGO, LIGO Scientific), *Phys. Rev. X* **13**, 011048 (2023), [arXiv:2111.03634 \[astro-ph.HE\]](#).
  - [26] B. P. Abbott *et al.* (LIGO Scientific, Virgo), *Phys. Rev. Lett.* **119**, 161101 (2017), [arXiv:1710.05832 \[gr-qc\]](#).
  - [27] C. Drischler, J. A. Melendez, R. J. Furnstahl, and D. R. Phillips, *Phys. Rev. C* **102**, 054315 (2020), [arXiv:2004.07805 \[nucl-th\]](#).
  - [28] C. Drischler, R. J. Furnstahl, J. A. Melendez, and D. R. Phillips, *Phys. Rev. Lett.* **125**, 202702 (2020), [arXiv:2004.07232 \[nucl-th\]](#).
  - [29] C. Drischler, S. Han, J. M. Lattimer, M. Prakash, S. Reddy, and T. Zhao, *Phys. Rev. C* **103**, 045808 (2021), [arXiv:2009.06441 \[nucl-th\]](#).

- [30] A. C. Sempowski, C. Drischler, R. J. Furnstahl, J. A. Melendez, and D. R. Phillips, (2024), [arXiv:2404.06323 \[nucl-th\]](#).
- [31] B. Hu *et al.*, *Nature Phys.* **18**, 1196 (2022), [arXiv:2112.01125 \[nucl-th\]](#).
- [32] B. T. Reed, R. Somasundaram, S. De, C. L. Armstrong, P. Giuliani, C. Capano, D. A. Brown, and I. Tews, (2024), [arXiv:2405.20558 \[astro-ph.HE\]](#).
- [33] P. T. H. Pang, L. Sivertsen, R. Somasundaram, T. Dietrich, S. Sen, I. Tews, M. W. Coughlin, and C. Van Den Broeck, *Phys. Rev. C* **109**, 025807 (2024), [arXiv:2308.15067 \[nucl-th\]](#).
- [34] C. Drischler, J. A. Melendez, R. J. Furnstahl, A. J. Garcia, and X. Zhang, *Front. in Phys.* **10**, 1092931 (2022), [arXiv:2212.04912 \[nucl-th\]](#).
- [35] E. Bonilla, P. Giuliani, K. Godbey, and D. Lee, *Phys. Rev. C* **106**, 054322 (2022), [arXiv:2203.05284 \[nucl-th\]](#).
- [36] J. Maldonado, R. J. Drischler, C. Furnstahl, and P. Mlinarić, “Greedy emulators for nuclear two-body scattering,” (2024), in preparation.
- [37] P. Giuliani, K. Godbey, E. Bonilla, F. Viens, and J. Piekarewicz, *Front. Phys.* **10** (2023), 10.3389/fphy.2022.1054524, [arXiv:2209.13039](#).
- [38] D. Odell, P. Giuliani, K. Beyer, M. Catacora-Rios, M. Y. H. Chan, E. Bonilla, R. J. Furnstahl, K. Godbey, and F. M. Nunes, *Phys. Rev. C* **109**, 044612 (2024), [arXiv:2312.12426 \[physics.comp-ph\]](#).
- [39] R. Essick, I. Tews, P. Landry, S. Reddy, and D. E. Holz, *Phys. Rev. C* **102**, 055803 (2020), [arXiv:2004.07744 \[astro-ph.HE\]](#).
- [40] Q. A. Huhn, M. E. Tano, J. C. Ragusa, and Y. Choi, *Journal of Computational Physics* **475**, 111852 (2023), [arXiv:2204.12006 \[math.NA\]](#).
- [41] J. H. Tu, C. K. Rowley, D. M. Luchtenburg, S. L. Brunton, and J. N. Kutz, *Journal of Computational Dynamics* **1**, 391 (2014).
- [42] J. N. Kutz, S. L. Brunton, B. W. Brunton, and J. L. Proctor, *Dynamic Mode Decomposition* (Society for Industrial and Applied Mathematics, Philadelphia, PA, 2016) <https://epubs.siam.org/doi/pdf/10.1137/1.9781611974508>.
- [43] S. L. Brunton, M. Budišić, E. Kaiser, and J. N. Kutz, “Modern koopman theory for dynamical systems,” (2021), [arXiv:2102.12086 \[math.DS\]](#).
- [44] N. Demo, M. Tezzele, and G. Rozza, *Journal of Open Source Software* **3**, 530 (2018).
- [45] S. Typel *et al.* (CompOSE Core Team), *Eur. Phys. J. A* **58**, 221 (2022), [arXiv:2203.03209 \[astro-ph.HE\]](#).
- [46] S. Lalit, A. C. Sempowski, and J. M. Maldonado (2024) <https://github.com/asempowski/SLM>.
- [47] J. Piekarewicz, “Neutron star matter equation of state,” in *Handbook of Supernovae*, edited by A. W. Alsabti and P. Murdin (Springer International Publishing, Cham, 2017) pp. 1075–1094.
- [48] I. Bombaci and D. Logoteta, *Astron. Astrophys.* **609**, A128 (2018), [arXiv:1805.11846 \[astro-ph.HE\]](#).
- [49] W.-C. Chen and J. Piekarewicz, *Phys. Lett. B* **748**, 284 (2015), [arXiv:1412.7870 \[nucl-th\]](#).
- [50] E. Chabanat, P. Bonche, P. Haensel, J. Meyer, and R. Schaeffer, *Nucl. Phys. A* **627**, 710 (1997).
- [51] V. Dexheimer, R. O. Gomes, T. Klähn, S. Han, and M. Salinas, *Phys. Rev. C* **103**, 025808 (2021).
- [52] V. Dexheimer and S. Schramm, *Astrophys. J.* **683**, 943 (2008), [arXiv:0802.1999 \[astro-ph\]](#).
- [53] A. Akmal, V. R. Pandharipande, and D. G. Ravenhall, *Phys. Rev. C* **58**, 1804 (1998).
- [54] L. McLerran and S. Reddy, *Phys. Rev. Lett.* **122**, 122701 (2019), [arXiv:1811.12503 \[nucl-th\]](#).
- [55] J. A. Melendez, C. Drischler, R. J. Furnstahl, A. J. Garcia, and X. Zhang, *J. Phys. G* **49**, 102001 (2022), [arXiv:2203.05528 \[nucl-th\]](#).
- [56] M. Korda and I. Mezić, *Journal of Nonlinear Science* **28**, 687 (2018).
- [57] P. J. Baddoo, B. Herrmann, B. J. McKeon, J. N. Kutz, and S. L. Brunton, “Physics-informed dynamic mode decomposition (pidmd),” (2021), [arXiv:2112.04307 \[math.DS\]](#).
- [58] M. Velegar, C. Keller, and J. N. Kutz, “Optimized dynamic mode decomposition for reconstruction and forecasting of atmospheric chemistry data,” (2024), [arXiv:2404.12396 \[cs.LG\]](#).
- [59] M. Sharak, A. Safavinejad, and M. Moayyedi, *Journal of Quantitative Spectroscopy and Radiative Transfer* **288**, 108248 (2022).
- [60] M. O. Williams, I. G. Kevrekidis, and C. W. Rowley, *Journal of NonLinear Science* **25**, 1307 (2015), [arXiv:1408.4408 \[math.DS\]](#).
- [61] See Supplemental Material at [URL will be inserted by publisher] for the mathematical formalism pertaining to both the Star Log-extended eMulator (SLM) and parametric extension (pSLM).
- [62] T. Lyons and A. D. McLeod, “Greedy recombination interpolation method (grim),” (2024), [arXiv:2205.07495 \[math.NA\]](#).
- [63] Bayesian Analysis of Nuclear Dynamics (BAND) Framework project (2020) <https://bandframework.github.io/>.

## Supplemental Material

Sudhanva Lalit <sup>1,\*</sup> Alexandra C. Sempowski <sup>2,†</sup> and Joshua M. Maldonado <sup>2,‡</sup>

<sup>1</sup>*Facility for Rare Isotope Beams, Michigan State University, East Lansing, MI 48824, USA*

<sup>2</sup>*Department of Physics and Astronomy and Institute of Nuclear and Particle Physics, Ohio University, Athens, OH 45701, USA*  
(Dated: November 21, 2024)

Supplemental material for the Letter, describing the scaling of the Tolman-Oppenheimer-Volkoff (TOV) equations, including tidal deformability, and the formalism of the Star Log-extended eMulation (SLM) method for both the logarithmic extension and the parametric algorithm. Particular care is given to describe the DMD algorithms upon which both emulators are based.

### SCALING TOV AND TIDAL EQUATIONS

The TOV equations [1, 2], along with the tidal deformability equation [3–5], are given by

$$\frac{dp}{dr} = -\frac{G}{c^2}(\epsilon(r) + P(r)) \frac{M(r) + 4\pi r^3 P(r)/c^2}{r(r - 2GM(r)/c^2)} \quad (1)$$

$$\frac{dm}{dr} = 4\pi r^2 \frac{\epsilon(r)}{c^2} \quad (2)$$

$$\frac{dy}{dr} = -\frac{y(r)^2}{r} - \frac{F(r)y(r)}{r} - \frac{Q(r)}{r} \quad (3)$$

where,

$$F(r) = \frac{1 - 4\pi Gr^2 (\epsilon(r) - P(r))/c^4}{1 - 2\frac{GM}{rc^2}} \quad (4)$$

and

$$Q(r) = \frac{4\pi Gr^2/c^4}{1 - 2\frac{GM}{rc^2}} \left( 5\epsilon(r) + 9p(r) + \frac{\epsilon(r) + p(r)}{c_s(r)^2} c^2 - \frac{6c^4}{4\pi r^2 G} \right) - 4 \left( \frac{G(M(r)/(rc^2) + 4\pi r^2 p(r)/c^4)}{1 - 2GM/(rc^2)} \right)^2 \quad (5)$$

where  $y(r) = \frac{R\beta(R)}{H(R)}$  and  $\beta = dH/dr^1$ .

Following closely Ref. [6], we use the scaling  $r = R_0 x$ ,  $M = M_0 m(x)$ ,  $P = P_0 p(x)$ ,  $\epsilon = \epsilon_0 \varepsilon(x)$ . To define the relevant scales, we set

$$\varepsilon_0 = P_0 \equiv \frac{1}{8\pi^2} \frac{(m_n c^2)^4}{(\hbar c)^3} \approx 1.285 \text{ GeV/fm}^3 \quad (6)$$

and adopt the natural normalization

$$\left[ \frac{2GM_0}{c^2 R_0} \right] = \left[ \frac{4\pi R_0^3 \varepsilon_0}{3M_0 c^2} \right] = 1. \quad (7)$$

Setting these quantities to unity, meaning to a dimensionless value of order one, establishes “natural” length and mass scales for the problem. This leads to

$$R_0 = \sqrt{\frac{3\pi}{\alpha_G}} \lambda_n \approx 8.378 \text{ km}, \quad (8)$$

$$M_0 = \left( \frac{R_0}{R_s^\odot} \right) M_\odot \approx 2.837 M_\odot, \quad (9)$$

where  $\alpha_G$  is the small, dimensionless gravitational coupling strength between two neutrons (or the neutron mass to Planck mass ratio),  $\lambda_n$  is the Compton wavelength of the neutron, and  $R_s^\odot$  represents the Schwarzschild radius of the Sun. Numerically, these values are:

$$\alpha_G = \frac{Gm_n^2}{\hbar c} \approx 5.922 \times 10^{-39} \quad (10)$$

$$\lambda_n = \frac{\hbar c}{m_n c^2} \approx 0.210 \times 10^{-18} \text{ km} \quad (11)$$

$$R_s^\odot = \frac{2GM_\odot}{c^2} \approx 2.953 \text{ km}. \quad (12)$$

The resulting scaled equations are given by

$$\frac{dp}{dx} = -\frac{1}{2} \frac{(\varepsilon(x) + p(x)) (m(x) + 3x^3 p(x))}{x^2 (1 - m(x)/x)} \quad (13)$$

$$\frac{dm}{dx} = 3x^2 \varepsilon(x) \quad (14)$$

$$\frac{dy}{dx} = -\frac{y(x)^2}{x} - \frac{F(x)y(x)}{x} - \frac{Q(x)}{x} \quad (15)$$

with

$$F(x) = \frac{1 - \frac{3}{2} (\varepsilon(x) - p(x))}{1 - \frac{m(x)}{x}},$$

and

$$Q(x) = \frac{\frac{3}{2}x^2}{\left(1 - \frac{m(x)}{x}\right)} \left[ 5\varepsilon(x) + 9p(x) + \frac{\varepsilon(x) + p(x)}{c_s^2(x)} - \frac{4}{x^2} \right] - \left( \frac{m(x)/x + 3x^2 p(x)}{\left(1 - \frac{m(x)}{x}\right)} \right)^2.$$

Solving these equations, we get  $m(x)$ ,  $p(x)$ ,  $y(x)$  as functions of  $x$ . To calculate the mass radius curve of a neutron star, one enforces the boundary condition that the pressure of star is zero at the surface. This enables one to find the mass and radius of the star for a given central pressure.

<sup>1</sup> For a detailed derivation of these equations, see Refs. [3–5].

We use  $y_R = y(r = R)$  where  $R$  is the radius of the star with mass  $M[M_\odot]$  to calculate the compactness of the star  $\beta = GM/R$ . Using this one can then calculate the dimensionless Love number  $k_2$  as

$$k_2 = \frac{8\beta^5}{5} (1 - 2\beta)^2 [2 + 2\beta(y_R - 1) - y_R] \\ \times \{2\beta(6 - 3y_R + 3\beta(5y_R - 8)) \\ + 4\beta^3 [13 - 11y_R + \beta(3y_R - 2) + 2\beta^2(1 + y_R)] \\ + 3(1 - 2\beta)^2 [2 - y_R + 2\beta(y_R - 1)] \log(1 - 2\beta)\}^{-1}. \quad (16)$$

## STAR LOG-EXTENDED EMULATION (SLM)

### Formalism

In this work, we closely follow Ref. [7] for the foundation of the SLM algorithm (see Alg. 1). Notably, italicized portions of the algorithm are direct extensions to Ref. [7]. We can express a nonlinear dynamical system using

$$\frac{\partial \mathbf{y}}{\partial r} = \mathcal{F}(\mathbf{y}(\mathbf{x}, r)) \quad (17)$$

where  $\mathcal{F}$  is a nonlinear operator governing the system's dynamics, which can be discretized in the phase space. This transforms the system into a system of coupled ordinary differential equations (ODEs)

$$\frac{d\mathbf{y}}{dr} = \mathbf{F}(\mathbf{y}(r), r), \quad (18)$$

where  $\mathbf{y} \in \mathbb{R}^N$  is a vector describing the system's state across  $N$  degrees of freedom at a given  $r$  and  $\mathbf{F}(\cdot)$  represents the dynamics in a discretized form.

Within the DMD framework, the nonlinear operator  $\mathbf{F}(\cdot)$  in Eq. (18) is replaced by a linear operator to model the evolution of the solution  $\mathbf{y}$ . This leads to the following surrogate system

$$\frac{d\mathbf{y}}{dr} = \hat{\mathbf{A}}\mathbf{y}, \quad (19)$$

which assumes that the data originates from linear dynamics. The operator  $\hat{\mathbf{A}}$  serves as a linear approximation and is identified through data-driven techniques. A series of snapshots is collected and the data is transformed by taking the logarithm, i.e.,  $\log \mathbf{X} = \log[\mathbf{y}_i]_{i=0}^m \in \mathbb{R}^{n \times m}$ .  $\log \mathbf{y}_r$  is a snapshot that represents the vector state at a given radial position  $r$ . We aim to find an operator  $\hat{\mathbf{A}} \in \mathbb{R}^{n \times n}$  such that

$$\log \mathbf{y}_{r+\delta r} = \hat{\mathbf{A}} \log \mathbf{y}_r, \quad (20)$$

where  $\log \mathbf{y}_r$ ,  $\log \mathbf{y}_{r+\delta r}$  are the two snapshots collected in consecutive radial positions. The operator  $\hat{\mathbf{A}}$  is a finite-dimensional approximation of the infinite-dimensional Koopman operator [8]. For simplicity, let  $\mathbf{z} = \log \mathbf{y}$ .

We then integrate machine learning techniques with SLM within the framework of the Koopman operator and its observables [9]. Inspired by support vector machines and kernel methods, in particular radial basis functions, a common approach for constructing the space  $\mathbf{X}$  is using a set of polynomials

$$X_j(\mathbf{y}) = \{y, y^2, y^3, \dots, y^n\}. \quad (21)$$

The goal is to select a sufficiently diverse set of observables, regardless of the specific feature space, to accurately approximate the Koopman operator. By choosing a broad set of candidate observables, we ensure that enough features are present to reconstruct the nonlinear system's underlying triplet pair accurately [8].

Given Koopman theory's flexibility with a broader set of observables, for SLM, we choose the set:

$$X_j(\mathbf{z}) = \{\mathbf{z}, \mathbf{z}^2\} \quad (22)$$

for polynomials in  $\mathbf{z}$ . This approach significantly enhances reconstruction and prediction capabilities of the data.

We then organize the snapshots in two matrices,  $\mathbf{X}^+$ ,  $\mathbf{X}^- \in \mathbb{R}^{n \times (m-1)}$ , defined as

$$\mathbf{X}^- = [\mathbf{z}_0 \ \mathbf{z}_1 \ \dots \ \mathbf{z}_{m-1} \ \mathbf{z}_0^2 \ \dots \ \mathbf{z}_i \mathbf{z}_j \ \dots \ \mathbf{z}_{m-1}^2], \\ \mathbf{X}^+ = [\mathbf{z}_1 \ \mathbf{z}_2 \ \dots \ \mathbf{z}_m \ \mathbf{z}_1^2 \ \dots \ \mathbf{z}_i \mathbf{z}_j \ \dots \ \mathbf{z}_m^2]. \quad (23)$$

The goal is to determine the matrix  $\mathbf{A}$  such that  $\mathbf{X}^+ \approx \mathbf{A}\mathbf{X}^-$ . Using the Moore-Penrose pseudoinverse we can find the best-fit operator  $\mathbf{A} = \mathbf{X}^+(\mathbf{X}^-)^\dagger$ . However, due to a high computational cost we opt for a more efficient method as in Ref. [7].

We begin by computing the singular value decomposition (SVD) of  $\mathbf{X}^- \approx \mathbf{U}\mathbf{\Sigma}\mathbf{V}^T$ , where  $\mathbf{U} \in \mathbb{C}^{n \times n}$  and  $\mathbf{V}^T \in \mathbb{C}^{m \times m}$  are two orthogonal matrices containing the principal modes of the system's solutions. The orthogonality of this matrix is crucial for ensuring that the algorithm identifies the correct modes for the reduced Koopman operator. The diagonal matrix  $\mathbf{\Sigma} \in \mathbb{C}^{n \times m}$  holds the singular values  $\sigma_i$ .

To reduce the computational complexity, we truncate the rank by selecting the first  $s$  columns of  $\mathbf{U}$  and  $\mathbf{V}$ , i.e.,  $\mathbf{U}_s \equiv [\mathbf{u}]_{i=1}^s \in \mathbb{C}^{n \times s}$  and  $\mathbf{V}_s \equiv [\mathbf{v}]_{i=1}^s \in \mathbb{C}^{m \times s}$ . Similarly, we form the diagonal matrix  $\mathbf{\Sigma}_s \equiv \text{diag}([\Sigma]_{i=1}^s) \in \mathbb{C}^{s \times s}$  by choosing the first  $s$  singular values. The rank  $s$  is selected to retain a sufficient amount of information, determined by

$$s = \text{argmin}_j \frac{\sum_{i=1}^j \sigma_i}{\sum_{i=1}^n \sigma_i}, \kappa \quad (24)$$

where  $\kappa$  is a value between 0 and 1 that is chosen by the user [7]. With the truncated SVD, we approximate

$$\mathbf{X}^- \approx \mathbf{U}_s \mathbf{\Sigma}_s \mathbf{V}_s^T. \quad (25)$$



---

**Algorithm 1: SLM**


---

- 1: Solve Eq. (20) and collect snapshots  $[\mathbf{y}_i]_{i=0}^m$  where  $i$  are the data indices.
  - 2: Compute the logarithm of these snapshots as  $[\log \mathbf{y}(r_i)]_{i=0}^m$ .
  - 3: Extend the snapshots by adding the Hadamard product of the arrays, i.e.  $\prod_{i,j} \log \mathbf{y}_i \log \mathbf{y}_j$ .
  - 4: Organize the snapshots in  $\mathbf{X}^+$  and  $\mathbf{X}^-$  data matrices.
  - 5: Perform SVD of  $\mathbf{X}^-$ :  $\mathbf{X}^- = \mathbf{U}\mathbf{\Sigma}\mathbf{V}^T$ .
  - 6: Keep  $s$  modes to desired accuracy and compute the reduced Koopman operator  $\mathbf{A}_s \equiv \mathbf{U}_s^T \mathbf{A} \mathbf{U}_s = \mathbf{U}_s^T \mathbf{X}^+ \mathbf{V}_s \mathbf{\Sigma}_s^{-1}$ .
  - 7: Perform eigen-decomposition of  $\mathbf{A}_s$  to obtain the reduced eigen-modes:  $\mathbf{A}_s \mathbf{W} = \mathbf{\Lambda} \mathbf{W}$ .
  - 8: Produce the full-state modes  $\mathbf{\Phi} = \mathbf{U}_s \mathbf{W}$ .
  - 9: Reconstruct the full coupled, *nonlinear* ODE solutions  $\mathbf{y}(r)$  using the first  $n$  modes with Eq. 28 and exponentiate the solutions.
- 

By utilizing the orthogonality of  $\mathbf{U}$  and  $\mathbf{V}$  and substituting this expression into Eq. (20), we derive the reduced Koopman operator in matrix form as

$$\mathbf{A}_s \equiv \mathbf{U}_s^T \mathbf{A} \mathbf{U}_s = \mathbf{U}_s^T \mathbf{X}^+ \mathbf{V}_s \mathbf{\Sigma}_s^{-1}. \quad (26)$$

The reduced matrix  $\mathbf{A}_s$  has dimensions  $s \times s$ , with  $s \ll n$ , significantly lowering the computational cost for the eigen-decomposition of  $\mathbf{A}_s \in \mathbb{C}^{s \times s}$ . The eigen-decomposition is given by:

$$\mathbf{A}_s \mathbf{W} = \mathbf{\Lambda} \mathbf{W}. \quad (27)$$

The projected modes are calculated using  $\mathbf{\Phi} = \mathbf{U}_s \mathbf{W}$ . Assuming  $\mathbf{y}$  consists of  $n$  solutions, we pick the first  $n$  modes from  $\mathbf{\Phi}$  to calculate reconstructed system by using

$$\mathbf{y}(l) = \mathbf{\Phi} \mathbf{\Lambda}^{l/\Delta l} \mathbf{b}_0 = \sum_i b_{0i} \phi_i(\lambda_i)^{l/\Delta l}, \quad (28)$$

where  $\mathbf{b}_0 = \mathbf{\Phi}^\dagger \mathbf{y}_0 \in \mathbb{R}^n$  is the vector of initial coefficients,  $\mathbf{\Phi}^\dagger$  is the pseudo-inverse of the matrix of modes, and  $\mathbf{y}_0 \in \mathbb{R}^n$  is the snapshot at the initial position,  $r = 0$ . In our case,  $l$  are integers as they are the index of the dataset, while  $\Delta l = 1$ .

### Parametric SLM (pSLM)

We expand upon the general algorithm for SLM presented in the previous section, in order to determine the evolution of the system under parametric dependence. This section also follows Ref. [7] closely, but for time-independent systems. The governing equations in Eq. (17) may involve specific parameters  $\mu$  allowing them to be reformulated in a parametric form

$$\frac{\partial \mathbf{y}^\mu}{\partial r} = \mathcal{F}(\mathbf{y}^\mu(\mathbf{x}, r; \mu), r; \mu). \quad (29)$$

After discretizing the phase space, this leads to a system of coupled parametric ordinary differential equations (ODEs):

$$\frac{d\mathbf{y}^\mu}{dr} = \mathbf{F}(\mathbf{y}^\mu(r; \mu), r; \mu). \quad (30)$$

In parametric SLM, the goal is to replace the nonlinear operator  $\mathbf{F}(\cdot)$  with a linear surrogate approximation

$$\frac{d\mathbf{y}^\theta}{dt} = \hat{\mathbf{A}}(\theta) \mathbf{y}^\theta, \quad (31)$$

where  $\theta$  is a vector of parameters corresponding to a prediction set.

In this work we utilize the reduced Eigen-Pair Interpolation (rEPI) technique proposed in [7]. Given a test parameter set  $\theta$ , individual classical SLMs are performed on a limited dataset. We then employ a greedy recombination interpolation method known as B-GRIM [10], to identify the nearest neighbor of the test parameter  $\theta$ . This enables a targeted interpolation of the eigen-pairs associated with the reduced Koopman operator. Using this approach, we compute SVD decompositions of  $J$  data sets and select the highest of the  $J$  ranks ( $s = \max_{j \in J}(s_j)$ ), yielding the reduced left- and right-singular matrices  $\mathbf{U}_{js}$  and  $\mathbf{V}_{js}^T$  along with the corresponding reduced singular value matrix  $\mathbf{\Sigma}_{js}$ . The individual reduced Koopman operators for each of the  $J$  cases are constructed as

$$\mathbf{A}_{js} = \mathbf{U}_{js}^T \mathbf{X}_j^+ \mathbf{V}_{js} \mathbf{\Sigma}_{js}^{-1}, \quad (32)$$

from which the reduced eigen-pairs are obtained as

$$\mathbf{A}_{js} \mathbf{W}_{js} = \mathbf{\Lambda}_{js} \mathbf{W}_{js}. \quad (33)$$

The desired test case eigen-pair  $(\mathbf{\Lambda}_{\theta s}, \mathbf{W}_{\theta s})$  is then determined using B-GRIM, leveraging the  $J$  eigen-pairs  $(\mathbf{\Lambda}_{js}, \mathbf{W}_{js})$ . Similarly,  $\mathbf{U}_{\theta s}$  and  $\mathbf{b}_\theta$  are computed through the same interpolation method. The projected modes are subsequently calculated as  $\mathbf{\Phi}_\theta = \mathbf{U}_{\theta s} \mathbf{W}_{\theta s}$ . Finally we obtain the solutions for the test parameter set  $\theta$  using Eq. (28) and keeping  $m$  modes. The corresponding full algorithm for pSLM is given in Alg. 2. As with Alg. 1, the italicized portions of this algorithm are direct extensions to Ref. [7].

### Banach greedy recombination interpolation method (B-GRIM)

In this approach [10], the goal is to find sparse approximations of functions thereby reducing computational

---

**Algorithm 2:** Parametric SLM

---

- ▷ Steps 1-7 are offline
- 1: Solve Eq. (29) for all training parameters  $\mu_j$  and collect  $N_s$  snapshots  $\mathbf{X}_{\mu_j} = [\mathbf{y}(r_i; \mu_j)]_{i=0}^m$  for  $1 \leq j \leq N_s$ .
  - 2: Compute the logarithm of these snapshots  $[\log \mathbf{y}(r_i; \mu_j)]_{i=0}^m$ .
  - 3: Extend the snapshots by adding the Hadamard product of the arrays, i.e.  $\left[ \prod_{i,k} \log \mathbf{y}_i \log \mathbf{y}_k \right]_j$ ,  $1 \leq j \leq J$ .
  - 4: Organize the snapshots in  $\mathbf{X}_j^+$  and  $\mathbf{X}_j^-$  data matrices,  $1 \leq j \leq J$ .
  - 5: Perform SVD of  $\mathbf{X}_j^-$ :  $\mathbf{X}_j^- = \mathbf{U}_j \mathbf{\Sigma}_j \mathbf{V}_j^T$ ,  $1 \leq j \leq J$ .
  - 6: Retain  $s$  modes and compute the reduced Koopman operator  $\mathbf{A}_{js} \equiv \mathbf{U}_{js}^T \mathbf{A} \mathbf{U}_{js} = \mathbf{U}_{js}^T \mathbf{X}_j^+ \mathbf{V}_{js} \mathbf{\Sigma}_{js}^{-1}$ ,  $1 \leq j \leq J$ .
  - 7: Perform the eigen-decomposition of  $\mathbf{A}_{js}$  to obtain the reduced eigen-modes as described in Eq. (33).
- ▷ Steps 8-11 are online
- 8: Interpolate SVD-modes  $\mathbf{U}_j$ , eigen-modes  $\mathbf{W}_{js}$ , and eigen-values  $\mathbf{\Lambda}_{js}$  to obtain  $\mathbf{U}_{\theta s}$ ,  $\mathbf{W}_{\theta s}$ , and  $\mathbf{\Lambda}_{\theta s}$ , respectively, using the B-GRIM interpolation method.
  - 9: Construct the modes  $\Phi_\theta = \mathbf{U}_{\theta s} \mathbf{W}_{\theta s}$ .
  - 10: Recover the initial coefficients  $\mathbf{b}_j$ ,  $1 \leq j \leq J$ .
  - 11: Reconstruct the full coupled set of solutions and exponentiate to obtain  $\mathbf{y}^\theta(r)$ .
- 

complexity. The method is composed of two main steps:  
 1) Banach extension and 2) Banach recombination.

#### Banach Extension

Let  $u \in \text{Span}(\mathcal{F})$  where  $\mathcal{F}$  is the set of functionals in the training set corresponding to features that approximate  $\mathbf{y}$ , and assume  $L \subset \Sigma$  be a finite collection of linear functionals, where  $\Sigma$  denotes the data. For each subset  $L \subset \Sigma$ , the method employs a recombination process to find an approximation  $u \in \text{Span}(\mathcal{F})$  for the target function  $\mathbf{y}$ , where  $\mathbf{y}$  represents the desired solution constrained by  $L$ . Typically this process introduces numerical errors; to minimize these, it is assumed that  $u$  is sufficiently close to  $\mathbf{y}$  at each functional  $\sigma \in L$ , a relationship that is formalized in the recombination step.

#### Banach recombination

Banach recombination phase consists of three steps.

1. Choose a subset  $L_j \subset \Sigma$  by randomly permuting the element order in  $L$ .
2. Perform recombination thinning to find an element  $u_j \in \text{Span}(\mathcal{F})$  that satisfies  $|\sigma(\mathbf{y} - u_j)| \leq \varepsilon_0$  for every  $\sigma \in L_j$ , where  $\varepsilon_0$  is a small tolerance value.
3. Compute the error metric  $E[u_j] := \max\{|\sigma(\mathbf{y} - u_j)| : \sigma \in \Sigma\}$ .

After identifying the elements  $u_1, \dots, u_s$ , define  $u$  as

$$u := \operatorname{argmin} E[w] : w \in \{u_1, \dots, u_s\} \quad (34)$$

This final  $u$  serves as the best approximation of the target function  $\mathbf{y}$ . The full algorithm and derivation of the method is provided in Ref. [10].

---

\* lalit@frib.msu.edu

† as727414@ohio.edu

‡ jm998521@ohio.edu

- [1] R. C. Tolman, Static Solutions of Einstein's Field Equations for Spheres of Fluid, *Physical Review* **55**, 364 (1939).
- [2] J. R. Oppenheimer and G. M. Volkoff, On Massive Neutron Cores, *Physical Review* **55**, 374 (1939).
- [3] T. Hinderer, Tidal Love numbers of neutron stars, *Astrophys. J.* **677**, 1216 (2008), [Erratum: *Astrophys. J.* 697, 964 (2009)], [arXiv:0711.2420 \[astro-ph\]](#).
- [4] T. Hinderer, B. D. Lackey, R. N. Lang, and J. S. Read, Tidal deformability of neutron stars with realistic equations of state and their gravitational wave signatures in binary inspiral, *Phys. Rev. D* **81**, 123016 (2010), [arXiv:0911.3535 \[astro-ph.HE\]](#).
- [5] S. Postnikov, M. Prakash, and J. M. Lattimer, Tidal Love Numbers of Neutron and Self-Bound Quark Stars, *Phys. Rev. D* **82**, 024016 (2010), [arXiv:1004.5098 \[astro-ph.SR\]](#).
- [6] J. Piekarewicz, Neutron star matter equation of state, in *Handbook of Supernovae*, edited by A. W. Alsabti and P. Murdin (Springer International Publishing, Cham, 2017) pp. 1075–1094.
- [7] Q. A. Huhn, M. E. Tano, J. C. Ragusa, and Y. Choi, Parametric dynamic mode decomposition for reduced order modeling, *Journal of Computational Physics* **475**, 111852 (2023), [arXiv:2204.12006 \[math.NA\]](#).
- [8] S. L. Brunton, M. Budišić, E. Kaiser, and J. N. Kutz, *Modern koopman theory for dynamical systems* (2021), [arXiv:2102.12086 \[math.DS\]](#).
- [9] J. N. Kutz, S. L. Brunton, B. W. Brunton, and J. L. Proctor, *Dynamic Mode Decomposition* (Society for Industrial and Applied Mathematics, Philadelphia, PA, 2016) <https://epubs.siam.org/doi/pdf/10.1137/1.9781611974508>.
- [10] T. Lyons and A. D. McLeod, Greedy recombination interpolation method (grim) (2024), [arXiv:2205.07495 \[math.NA\]](#).